

Secondary resonances and the boundary of effective stability of Trojan motions

Rocío Isabel Páez¹ and Christos Efthymiopoulos¹

¹Research Center for Astronomy and Applied Mathematics, Academy of Athens

Abstract:

One of the most interesting features in the libration domain of co-orbital motions is the existence of secondary resonances. For some combinations of physical parameters, these resonances occupy a large fraction of the domain of stability and rule the dynamics within the stable tadpole region. In this work, we present an application of a recently introduced ‘basic Hamiltonian model’ H_b for Trojan dynamics [33], [35]: we show that the inner border of the secondary resonance of lowermost order, as defined by H_b , provides a good estimation of the region in phase-space for which the orbits remain regular regardless the orbital parameters of the system. The computation of this boundary is straightforward by combining a resonant normal form calculation in conjunction with an ‘asymmetric expansion’ of the Hamiltonian around the libration points, which speeds up convergence. Applications to the determination of the effective stability domain for exoplanetary Trojans (planet-sized objects or asteroids) which may accompany giant exoplanets are discussed.

1 Introduction

Despite the theoretical possibility of the existence of Trojan exoplanets ([18], [1], [3]), no such body has been identified so far in exoplanet surveys. This lack of identification may reflect formation constrains, constrains to detectability ([17], [4], [19], [20], [21]), or it may simply be due to stability reasons. In this framework, the question of ‘effective stability’, i.e. stability of the orbit of a Trojan body for times as long as a considerable fraction of the age of the hosting system, comes to the surface. The question of effective stability has been addressed nearly exhaustively in the case of Trojan asteroids in our Solar System (see, for example, [27], [22], [15], [39], [37], [23], [5], [24]) from both numerical and analytical approaches, but only scarcely in the case of exoplanetary systems (see [30], [12], [38], [9]). One main reason for the scarcity of results in this latter case is the vast volume of parameter space to be investigated, in conjunction with the multi-body nature of the problem: to determine the long-term stability of Trojan motions becomes essentially a problem of secular dynamics with as many degrees of freedom as the number of planets in the system under consideration. Any attempt to face the problem other than numerical simulation clearly requires a simplification of the dynamical model, without this leading to oversimplified conclusions regarding the long-term orbital stability.

In the present work, we discuss a key property of the dynamics induced by *secondary resonances* in the domain of Trojan motions, which in addition to its own proper interest, can serve also the purpose of obtaining a simple analytical estimate of the effective stability boundary of Trojan motions in hypothetical exoplanetary systems. Our analysis of the resonant dynamics stems from a set of considerations or assumptions, whose validity can be most easily judged by comparison with some results and figures of a previous work of ours ([33]) as follows:

1) In [33] we provided a formalism of the problem of the dynamics of Trojan bodies in the Hamiltonian context, which recovers all essential features as discovered in previous literature ([10], [11], [28], [29]); preceding works, however, focus mostly on a direct investigation of the equations of motion, averaged or not with respect to short period terms. In our works we stressed, instead, a main advantage of the new formalism, namely the allowance to recruit the full machinery of Hamiltonian methods in order to better analyze the problem under study.

2) We investigated the features of Trojan dynamics which hold under three physically relevant assumptions: i) that the motions of all planets, including the Trojan body, are close to planar, ii) that the Trojan body is small enough to be considered as test particle, in agreement with formation scenaria which suggest that exo-Trojans should be at most Mars-sized objects ([1]), and iii) that the

arXiv:1712.08460v1 [astro-ph.EP] 22 Dec 2017

secular dynamics of the hosting system is such that the eccentricity vector of the primary companion of the Trojan body undergoes circulation with a nearly constant frequency g' , and has a length which undergoes variations around some non-zero value e_0 .

Under assumptions (i) to (iii), we find that the Hamiltonian of motion of the Trojan body, averaged over short period terms for the motions of the remaining planets, can be decomposed in the form $H = H_b + H_{sec}$ where: H_b , called the ‘basic model’, describes short period and synodic motions, and yields a constant proper eccentricity for the Trojan body, and H_{sec} contains all remaining secular perturbations. Furthermore H_b has a universal form, i.e., it suffices to redefine the physical meaning of the angular canonical variables, to keep its form unaltered in the whole hierarchy of restricted problems (circular, elliptic, secular with more than one perturbing planets).

3) The decomposition $H = H_b + H_{sec}$ leads to a specific physical understanding of the dynamics when the primary planet has a mass in the giant planet range. In this case, the three timescales related to the short-period, synodic and secular motions have a separation by about one or less order of magnitude from each other. Then, due to the specific features of H_b described above, we arrive at the following key remark: the model H_b produces, in phase space, a set of secondary resonances corresponding to commensurabilities between the frequencies of the short-period and synodic motions ([13]). It is easy to see that these are the only secondary resonances which occupy a non-zero volume in phase space in the whole hierarchy of restricted problems that one could use as dynamical models for the Trojan body. However, there exists a *modulation* effect ([2]) due to the influence of H_{sec} on this set of secondary resonances: the separatrices pulsate slowly (with one or more secular frequencies) and, as a result, in the ‘domain of uncertainty’ ([31]) created by such pulsations, the motions become chaotic. Such an effect is possible to visualize already in the Elliptic Restricted Three-Body Problem, namely the simplest model with non trivial H_{sec} . The reader is referred to Figures 5 to 15 of [33] which show in detail the statements below, by exemplifying the outcome of the modulation effects for the secondary resonances 1:5 up to 1:12, when the modulus of the eccentricity vector e_0 of the primary companion varies from $e_0 = 0$ to just a moderate value $e_0 = 0.1$. By inspecting the stability maps in the space of the Trojan body’s proper elements, one sees that, for e_0 slightly larger than zero, the separatrix pulsation for the secondary resonances becomes large enough so as to wipe out nearly completely the domain of stable motions occupied by such resonances. As a result, the only remaining stable motions are those in a inner (closer to the libration center) domain devoid of secondary resonances. In fact, as found in many works (e.g. [37], [26]) there can still be resonances involving one or more secular frequencies which penetrate this innermost stability domain. However, since these resonances are thin and typically do not overlap, they can only induce a very slow chaotic diffusion of the Arnold type, which can be neglected for all practical purposes. Hence, the innermost domain, devoid of the secondary resonances of H_b , meets all criteria of effective stability, and, indeed, stability maps indicate the robustness of this domain against variations of the orbital parameters of the Trojan body.

1.1 Summary of the method

Stemming from remarks (1) to (3) above, we propose below a practical method to define the effective stability domain of Trojan motions. This is based on the following steps:

Step 1: analyze a given system where hypothetical Trojan bodies are sought for and compute the Hamiltonian H_b ,

Step 2: identify the largest in size (typically lowest in order) secondary resonance of H_b for given parameter values,

Step 3: compute a resonant normal form and evaluate the theoretical separatrices of the identified secondary resonance,

Step 4: assume that all stable domains of resonant motions extending beyond the innermost (closest to the libration center) branch of the theoretical separatrices were wiped out by secular modulation effects.

Then, the locus S formed by the intersection of the family of all computed innermost theoretical separatrices, along the dominant secondary resonance, with any chosen (with respect to phases) plane PP of Trojan proper elements, yields the boundary of the effectively stability domain in the plane PP .

The above computation is fast and straightforward to perform with modern computer algebra programs, and thus competitive to large grid computations of effective stability maps. In our own implementation we use the normal form method adopted in [34], [35].

In the rest of the paper, we discuss both the dynamical role of the secondary resonances in delimiting the main domain of effective stability as well as our particular analytical method of computing the border of this domain. The structure of the paper is as follows: In Section 2, we review the derivation and features of the Hamiltonian H_b , as well as our way to expand H_b in a form suitable for resonant normal form computations. A novel feature is the adoption of an ‘asymmetric expansion’ which improves convergence. Section 3 explains in detail the realization of the *Steps 1-4*, in particular the computation of the theoretical separatrices of the dominant secondary resonance and their superposition to stability maps in the space of proper elements. Section 4 contains the main results: (a) we provide numerical evidence, based on stability maps, of how the separatrices of the secondary resonances of the ‘basic model’ H_b act as delimiters of the effective stability domain; (b) we use an analytical method to estimate this boundary; (c) we discuss the robustness of the present approach against changing the model’s parameters (masses and eccentricities), as well as when considering, in the numerical integrations, the full three-body problem instead of the ERTBP. Section 5 summarizes our main conclusions.

2 Basic Hamiltonian H_b and its asymmetric expansion

2.1 Main features of the basic model H_b

In [33], a Hamiltonian formulation was provided for the Trojan motion which applies to the planar Elliptic Restricted Three-Body Problem (ERTBP) with a central mass, a primary perturber or simply ‘primary’, and the Trojan test particle, or when S additional perturbing bodies are present but far from MMRs, the so-called ‘Restricted Multi-Planet Problem’ (RMPP)). The Hamiltonian reads

$$H = H_b(Y_f, \phi_f, u, v, Y_p; \mu, e'_0) + H_{sec}(Y_f, \phi_f, u, v, Y_p, \phi, Y_1, \phi_1, \dots, Y_S, \phi_S) . \quad (1)$$

In Eq. (1), the variables (ϕ_f, Y_f) , (u, v) and (ϕ, Y_p) are pairs of action-angle variables, whose definition stems from Delaunay-like variables following a sequence of four consecutive canonical transformations (see Appendix A). In particular, (Y_f, ϕ_f) are action-angle variables describing the fast degree of freedom, of frequency

$$\omega_f \equiv \dot{\phi}_f = 1 - \frac{27}{8} \mu + g' + \dots , \quad (2)$$

where g' is fundamental frequency of precession of the primary’s perihelion. The pair (u, v) describe the particle’s synodic librations, $u \simeq \lambda - \lambda' - \pi/3$, $v \simeq \sqrt{a} - 1$, with λ, λ' the mean longitudes of the test particle and of the primary, a the particle’s major semi-axis, and $a' = 1$. The associated frequency at the libration center is

$$\omega_s \equiv \dot{\phi}_s = -\sqrt{\frac{27\mu}{4}} + \dots . \quad (3)$$

Finally, the secular motion of the test particle’s eccentricity vector $(e \cos(\omega - \omega'), e \sin(\omega - \omega'))$, where e is the eccentricity and ω, ω' are the arguments of the perihelion of the test particle and the primary respectively, is described by a circulation around the forced equilibrium point, given in our variables by a set of action angle variables (Y_p, ϕ) . The associated secular frequency is

$$g \equiv \dot{\phi} = \frac{27}{8} \mu - g' + \dots . \quad (4)$$

We call the term H_b in the Hamiltonian of Eq. (1) the ‘basic Hamiltonian model’ for Trojan motions in the 1:1 MMR. Its detailed form is given in the Supplementary Online Material of [33]. We find

$$H_b = -\frac{1}{2(1+v)^2} - v + (1+g')Y_f - g'Y_p - \mu \mathcal{F}^{(0)}(u, \phi_f, v, Y_f - Y_p; e'_0) . \quad (5)$$

The physical parameters entering into H_b are i) the mass parameter $\mu = \frac{m'}{m'+M}$, where M is the mass of the central mass and m' the mass of the primary, ii) the mean value of the length of the eccentricity vector of the heliocentric orbit of the primary perturber, e'_0 . In the ERTBP, one has simply $e' = e'_0$, $g' = 0$ (implying also $\omega' \equiv \text{const}$). However, the form of H_b remains the same in both the ERTBP and the RMPP. In particular, the angle ϕ is defined via a ‘shift transformation’ depending only on the relative difference $\Delta\omega = \omega - \omega'$. Physically, the secular dynamics induced under H_b appears the same in the ERTBP and in the RMPP, when, in the latter case, it is viewed in apsidal co-rotation with the primary. Furthermore, since the angle ϕ is ignorable in H_b , the action variable Y_p is an integral of the basic Hamiltonian. Then, the ERTBP and the RMPP are diversified only by their different form of the functions H_{sec} . In particular, in the RMPP case H_{sec} contains also pairs of action angle variables associated with the secular precessions of the S additional bodies, while in the ERTBP it contains only the angle ϕ associated with the secular precession of the test particle. Finally, H_{sec} disappears all together in the circular RTBP. Thus, H_b becomes the exact Hamiltonian in this case. Note, however, that in the ERTBP H_b is *not* equal to the ensemble of all terms independent of e' .

The basic model H_b represents a drastic reduction of the number of degrees of freedom with respect to the original problem. In the sequel, we will focus on one particular feature of H_b , namely the presence of *secondary resonances*, which correspond to commensurability relations between ω_f and ω_s . In particular, we focus on the role of these resonances in practically determining the boundary of the effective domain of stability for the Trojan motions.

2.2 Asymmetric expansion

The resonant normal form computed in Section 3 below provides a model for studying the dynamics within or near a secondary resonance of the form:

$$m_f\omega_f + m_s\omega_s = 0 . \quad (6)$$

A *non-resonant* normal form for the model H_b , allows to find the location of secondary resonances in a space of suitably defined proper elements for the Trojan body (see [35]). However, the non-resonant normal form does not allow to compute the local phase portrait, i.e., the separatrices associated with each resonance. Furthermore, all series expansions which are polynomial in the variables u, v exhibit poor convergence, a fact associated with the singularity (collision with the primary) at $u = -\pi/3$. In order to deal with this problem, a *partially expanded* version of the H_b can be used [34], in which all the powers of the quantity $\beta(\tau) = \frac{1}{\sqrt{2-2\cos\tau}}$ (with $\tau = u + \pi/3$) are kept unexpanded. This leads to a Hamiltonian of the form

$$H_b(v, \mathcal{Y}, \tau, \phi_f, Y_p) = -v + \sum_{i=0}^{\infty} (-1)^{i-1} (i+1) \frac{v^i}{2} + \mathcal{Y} + Y_p \\ + \mu \sum_{\substack{m_1, m_2, m_3 \\ k_1, k_2, k_3, j}} a_{m_1, m_2, m_3, k_1, k_2, j} e^{ik_3 v^{m_1}} \cos^{k_1}(\tau) \sin^{k_2}(\tau) \mathcal{Y}^{m_4} \cos^{m_2} \phi_f \sin^{m_3} \phi_f \beta^j(\tau) , \quad (7)$$

where $\tau = u + \pi/3$, $\mathcal{Y} = Y_f - Y_p$, and $a_{m_1, m_2, m_3, k_1, k_2, j}$ are rational numbers.

The librations in τ (or u) are represented in terms of the synodic angle variable ϕ_s , i.e., the phase of the synodic libration. The computation of a resonant normal form requires to explicitly Fourier expand the terms of H_b in *both* angles ϕ_f and ϕ_s . Although the Hamiltonian (7) represents a Fourier expansion for the fast d.o.f. (angle ϕ_f), there still remain the powers of β that must be expanded in powers of u in order to obtain a complete Fourier expansion in the angle ϕ_s as well. Due to the singularity at $\tau = 0$ (or $u = -\pi/3$), any Taylor expansion of the functions $\beta(\tau)^N = \frac{1}{(2-2\cos\tau)^{N/2}}$, with $N \in \mathbb{N}$, around a certain τ_0 is convergent only in the domain $\mathcal{D}_{\tau_0, \delta}$ centered at τ_0 and of radius $\delta = \text{Min}\{\tau_0, 2\pi - \tau_0\}$. The most common approach consists of Taylor expansions around the libration equilibrium point, located at $\tau_0 = \frac{\pi}{3}$, for L4, or $\tau_0 = \frac{5\pi}{3}$ for L5. The corresponding δ in this case is $\frac{\pi}{3}$. One finds that many Trojan orbits, and important secondary resonances, may cross this domain. In such cases, the resonant normal form construction is obstructed by the poor convergence of the original Hamiltonian expansion.

In order to face this problem, we find a different polynomial representation of the Hamiltonian H_b in the variables (u, v) by performing an *asymmetric* expansion, i.e. expansion around a *non-equilibrium point* $\tau_0 \neq \pi/3$, selected to be further away from the singularity but close enough to the libration point, so that a re-ordering of the expansion in powers of u yields a negligible term linear in u (since $u = 0$ represents the equilibrium point of H_b). Here we choose $\tau_0 = \frac{\pi}{2}$. In this case, we obtain a polynomial expansion of the Hamiltonian in powers of the quantity $(\tau - \pi/2)$. Re-ordering the terms, we express it as a polynomial in powers of u . It is immediate to see that any finite truncation of this expression yields a different polynomial than the one obtained by a finite truncation of the direct Taylor expansion around $\tau = \pi/3$. However, the new expression better represents the quantities $\beta(\tau)^N$ in a domain extended up to $\tau \sim \pi$. We call the expansion around $\tau_0 = \frac{\pi}{2}$ *asymmetric*, while the one around $\tau_0 = \frac{\pi}{3}$ *symmetric*.

Figure 1 shows the benefits of the asymmetric expansion when compared to the symmetric one. We consider the functions

$$\begin{aligned} B_1(\tau) &= \frac{\cos \tau}{\beta(\tau)} = \frac{\cos \tau}{(2 - 2 \cos \tau)^{1/2}}, & B_3(\tau) &= \frac{\cos \tau}{\beta^3(\tau)} = \frac{\cos \tau}{(2 - 2 \cos \tau)^{3/2}}, \\ B_5(\tau) &= \frac{\cos \tau}{\beta^5(\tau)} = \frac{\cos \tau}{(2 - 2 \cos \tau)^{5/2}}, & B_7(\tau) &= \frac{\cos \tau}{\beta^7(\tau)} = \frac{\cos \tau}{(2 - 2 \cos \tau)^{7/2}}, \end{aligned} \quad (8)$$

which represent the most common terms in powers of $\beta(\tau)$ appearing in Eq. (7). The symmetric Taylor expansion of B_1 , B_3 , B_5 and B_7 around $\tau_0 = \pi/3$ yield the polynomials

$$B_{M,\pi/3}(u) = B_M(\pi/3) + B_M^{(1)}(\pi/3)u + \frac{1}{2}B_M^{(2)}(\pi/3)u^2 + \frac{1}{6}B_M^{(3)}(\pi/3)u^3 + \dots, \quad (9)$$

where $B_M^{(n)}(\pi/3)$ is the n -th derivative of the function B_M , evaluated at $u = \pi/3$, $M = 1, 3, 5, 7$ and $u = \tau - \pi/3$. On the other hand, the asymmetric Taylor expansions of the same functions around $\tau_0 = \pi/2$ yield the polynomials

$$B_{M,\pi/2}(u) = B_M(\pi/2) + B_M^{(1)}(\pi/2)\left(u - \frac{\pi}{6}\right) + \frac{1}{2}B_M^{(2)}(\pi/2)\left(u - \frac{\pi}{6}\right)^2 + \frac{1}{6}B_M^{(3)}(\pi/2)\left(u - \frac{\pi}{6}\right)^3 + \dots. \quad (10)$$

Fig. 1 compares the graphs of the original functions $B_M(u)$ (pink) with the two corresponding expansions $B_{M,\pi/3}(u)$ (symmetric, blue) and $B_{M,\pi/2}(u)$ (asymmetric, green) up to order 10 in u . We see that both expansions provide a good representation of the original function up to a certain extent in u , but for increasing values of u , the asymmetric expansions are more accurate than the symmetric ones in a domain extending to higher values of u . The improvement in accuracy is more notorious as M increases. In fact, we find that the polynomial approximations to H_b found by the asymmetric expansion is accurate up to $u \sim 1$ rad, which is enough to cover the effective stability domain in most physically relevant parameter values. Only very close to $u \sim 0$, the symmetric expansion is marginally more accurate than the asymmetric one. This yields a slight shift of the equilibrium point of H_b with respect to $u = 0$, typically of about $\sim 10^{-8}$ rad, i.e. practically negligible.

Similar results are found for the asymmetric and symmetric expansions of the functions $\frac{\sin \tau}{\beta(\tau)}$ appearing in H_b . Finally, the asymmetric expansions for both types of functions can be easily performed by a closed set of formulas, given in the Appendix B.

3 Resonant normal form

3.1 Hamiltonian preparation

The construction of the asymmetrically expanded H_b consists of two steps: i) replacement of the expansions for the variables (u, v) in Eq. (7), and ii) transformation to action-angle variables.

In order to replace the polynomial truncations for the functions of Eq. (8) into Eq. (7), we adopt the asymmetric expansion (10), using the formulæ provided in the Appendix B. Regarding v , it is enough to consider the Taylor expansion of H_b with respect to v around zero. The maximum

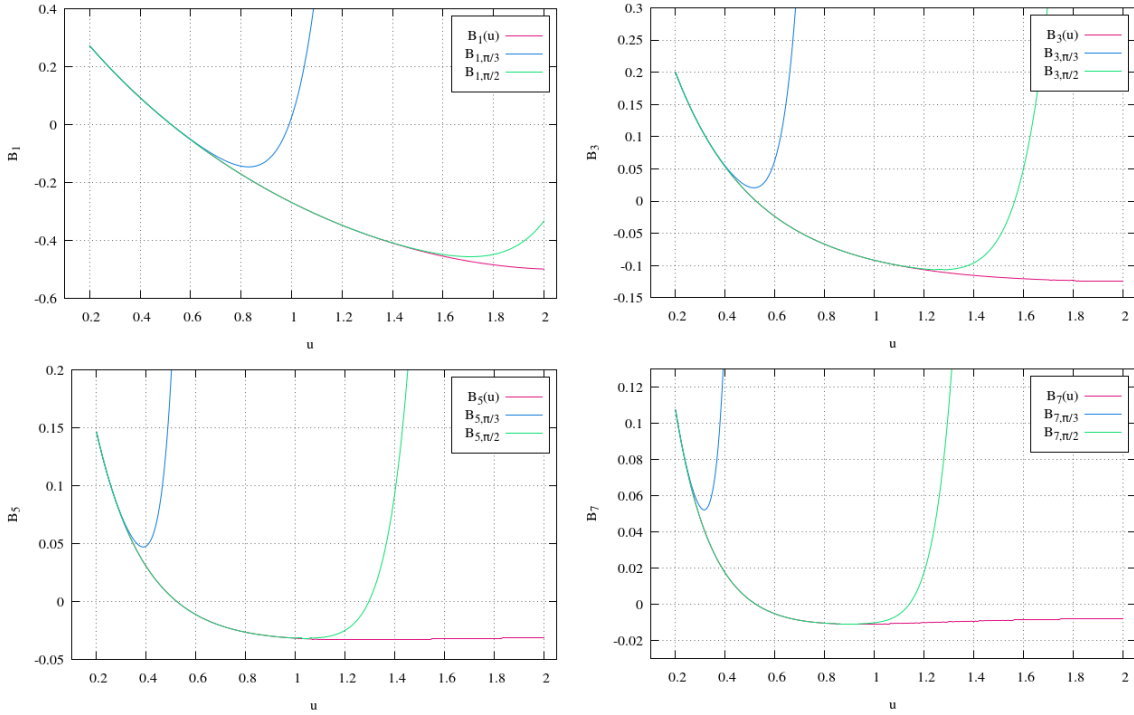


Figure 1: Comparison of the functions $B_M(u)$ (pink), with the expansions $B_{M,\pi/3}(u)$ (blue) and $B_{M,\pi/2}(u)$ (green), up to order 10 in u , for $M = 1, 3, 5, 7$ and $u \in [0.2, 2]$.

truncation order is determined in terms of a ‘book-keeping parameter’ ([8]; see below). After these replacements, the Hamiltonian H_b takes the form

$$H_b(v, \mathcal{Y}, u, \phi_f, Y_p) = Y_p + \sum_{\substack{m_1, m_2, \\ m_3, m_4}} \mathbf{a}_{m_1, m_2, m_3, m_4} v^{m_1} u^{m_2} (\sqrt{\mathcal{Y}})^{m_3} \cos(m_4 \phi_f), \quad (11)$$

where the real coefficients $\mathbf{a}_{m_1, m_2, m_3, m_4}$ depend on the parameters μ and e'_0 (or simply e' in the ERTBP).

Next, we diagonalize H_b in order to obtain a harmonic oscillator quadratic part for the synodic degree of freedom. Diagonalization is performed by the linear canonical transformation $(u, v) \rightarrow (U, V)$ defined by the set of formulas:

$$\begin{pmatrix} u \\ v \end{pmatrix} = \frac{1}{\sqrt{\text{Det}(\mathbf{E})}} (\mathbf{E} \cdot \mathbf{B}) \begin{pmatrix} U \\ V \end{pmatrix}, \quad \mathbf{B} = \begin{pmatrix} \frac{1}{\sqrt{2}} & \frac{-i}{\sqrt{2}} \\ \frac{-i}{\sqrt{2}} & \frac{1}{\sqrt{2}} \end{pmatrix}, \quad (12)$$

where \mathbf{E} is a 2×2 matrix with columns any two eigenvectors $e_{1,2}$ associated with the eigenvalues $\lambda_{1,2} = \pm \omega_s$ of the matrix \mathbf{M}

$$\mathbf{M} = \begin{pmatrix} \mathbf{a}_{(1,1,0,0)} & 2\mathbf{a}_{(2,0,0,0)} \\ -2\mathbf{a}_{(0,2,0,0)} & -\mathbf{a}_{(1,1,0,0)} \end{pmatrix}. \quad (13)$$

From the variables U and V we then pass to the action-angle variables (\mathcal{Y}, ϕ_f) with

$$U = \sqrt{2Y_s} \sin \phi_s, \quad V = \sqrt{2Y_s} \cos \phi_s. \quad (14)$$

The last step corresponds to a re-organization of the terms of the Hamiltonian, according to a *book-keeping* parameter [8]. This is a parameter with numerical value equal to $\epsilon = 1$. To every term in the Hamiltonian (11), we assign a power of ϵ indicating the order of the normalization at which the term will be treated. Thus, coefficients with powers of ϵ propagate throughout the series at all normalization steps, helping to organize the terms in different orders of smallness. Regarding the original Hamiltonian, we adopt the following book-keeping rule:

Rule 3.1 *To every monomial of the type*

$$\mathbf{c}_{(k_1, k_2, k_3, k_4)} (\sqrt{Y_s})^{k_1} (\sqrt{\mathcal{Y}})^{k_2} \frac{\cos}{\sin} (k_3 \phi_s + k_4 \phi_f) ,$$

assign a book-keeping coefficient $\epsilon^{r(k_1, k_2, k_4)}$, where the exponent $r(k_1, k_2, k_4)$ is given by

$$r(k_1, k_2, k_4) = \begin{cases} \text{Max}(0, k_1 + k_2 - 2) & \text{if } k_4 = 0 \\ \text{Max}(0, k_1 + k_2 - 2) + 1 & \text{if } k_4 \neq 0 \end{cases} .$$

This book-keeping rule ensures also that the terms of zero-th order in ϵ are linear in \mathcal{Y} and Y_s . The Hamiltonian now takes the form:

$$\begin{aligned} H_b(Y_s, \mathcal{Y}, \phi_s, \phi_f, Y_p) &= Y_p + \omega_s Y_s + \omega_f \mathcal{Y} \\ &+ \sum_{r=1}^{r_{max}} \mathbf{c}_{(k_1, k_2, k_3, k_4)} \epsilon^r (\sqrt{Y_s})^{k_1} (\sqrt{\mathcal{Y}})^{k_2} \frac{\cos}{\sin} (k_3 \phi_s + k_4 \phi_f) . \end{aligned} \quad (15)$$

From the canonical transformation in Eq. (14), it is straightforward to check that the harmonics of the angles ϕ_f and ϕ_s have the same parity as the powers of the corresponding functions in the variables $\sqrt{\mathcal{Y}}$ and $\sqrt{Y_s}$.

3.2 Resonant normalization

The resonant normalization of the Hamiltonian (15) consists of a sequence of near-identity canonical transformations, in ascending powers of the book-keeping parameter ϵ , aiming to eliminate from the Hamiltonian the trigonometric dependence on the angles in any linear combination other than the one which corresponds to the selected secondary resonance (Eq. 6). The resulting normal form includes, besides terms depending just on the actions, also terms of the form

$$b(\mathbf{p}^{(r)}) e^{i(\mathbf{k} \cdot \mathbf{q}^{(r)})} . \quad (16)$$

Here, $\mathbf{q}^{(0)} = (\phi_f, \phi_s)$, $\mathbf{p}^{(0)} = (\mathcal{Y}, Y_s)$, and the superscript (r) indicates the variables found after r consecutive near-identity normalizing transformations of $(\mathbf{q}^{(0)}, \mathbf{p}^{(0)})$. Also, $\mathbf{k} = (k_1, k_2)$ belongs to the set \mathcal{M} called the resonant module (Eq. 17 below). The terms (16) allow to determine the theoretical separatrices of the secondary resonance via the process described in subsection 3.3 below.

The general recursive resonant normalization algorithm is defined as follows: Let m_1, m_2 be two integers marking the secondary resonance $\frac{m_1}{m_2} \approx \frac{\omega_f}{\omega_s}$. The resonant module \mathcal{M} is the set of integer vectors defined by

$$\mathcal{M} = \{\mathbf{k} = (k_1, k_2) : k_1 m_1 + k_2 m_2 = 0\} , \quad (17)$$

where $\sum_{i=1}^2 |m_i| \neq 0$.

Let us assume that the Hamiltonian is in normal form up to order r in the book-keeping parameter, i.e.

$$\mathcal{H} = \mathcal{Z}_0 + \epsilon \mathcal{Z}_1 + \dots + \epsilon^r \mathcal{Z}_r + \epsilon^{r+1} \mathcal{H}_{r+1}^{(r)} + \epsilon^{r+2} \mathcal{H}_{r+2}^{(r)} + \dots . \quad (18)$$

From the terms of order ϵ^{r+1} , in the Fourier expansion,

$$\mathcal{H}_{r+1}^{(r)} = \sum_{\mathbf{k}} b(\mathbf{p}^{(r)}) e^{i(\mathbf{k} \cdot \mathbf{q}^{(r)})} , \quad (19)$$

where we isolate the terms that we want to eliminate in the present step, denoted by

$$*\mathcal{H}_{r+1}^{(r)} = \sum_{\mathbf{k} \notin \mathcal{M}} b(\mathbf{p}^{(r)}) e^{i(\mathbf{k} \cdot \mathbf{q}^{(r)})} . \quad (20)$$

The homological equation

$$\epsilon^{r+1} *\mathcal{H}_{r+1}^{(r)} + \{\mathcal{Z}_0, \chi_{r+1}\} = 0 \quad (21)$$

has the solution

$$\chi_{r+1} = \epsilon^{r+1} \sum_{\mathbf{k} \notin \mathcal{M}} \frac{b(\mathbf{p}^{(r)})}{i(\mathbf{k} \cdot \boldsymbol{\omega})} e^{i(\mathbf{k} \cdot \mathbf{q}^{(r)})}, \quad (22)$$

with $\boldsymbol{\omega} = (\omega_f, \omega_s)$.

Having the expression of the generating function, we compute the transformed Hamiltonian

$$\mathcal{H}^{(r+1)} = \exp(\mathcal{L}_{\chi_{r+1}}) \mathcal{H}^{(r)}, \quad (23)$$

where

$$\exp(\mathcal{L}_\chi) \cdot = \mathbb{I} \cdot + (\mathcal{L}_\chi \cdot) + \frac{1}{2} (\mathcal{L}_\chi^2 \cdot) + \dots \quad (24)$$

and the *Lie operator* $\mathcal{L}_\chi \equiv \{\cdot, \chi\}$ ($\{\cdot, \cdot\}$ denotes the Poisson bracket).

By construction, the Hamiltonian in Eq. (23) is in normal form up to order ϵ^{r+1} , i.e.

$$\mathcal{H} = \mathcal{Z}_0 + \epsilon \mathcal{Z}_1 + \dots + \epsilon^r \mathcal{Z}_r + \epsilon^{r+1} \mathcal{Z}_{r+1} + \epsilon^{r+2} \mathcal{H}_{r+2}^{(r)} + \epsilon^{r+3} \mathcal{H}_{r+3}^{(r)} + \dots \quad (25)$$

3.3 Computation of theoretical separatrices

Let us consider the function H_b given in Eq. (15) as the starting Hamiltonian $H_b^{(0)}$ of the normalizing scheme. We apply the normalizing scheme presented above, up to a maximum normalization order R in ϵ . In the examples that follow, the maximum normalization order examined was $R = 22$. However, since the resonant normal form series are asymptotic, depending on the parameters and resonance considered, the optimal normalization order (yielding the minimum remainder as computed e.g. in [7]) varies, yielding optimal orders between $R = 14$ and $R = 20$.

Let $H_b^{(R)}$ be the final normalized Hamiltonian. According to Eq. (16), the form of $H_b^{(R)}$ is given by

$$H_b^{(R)} = \sum_{\substack{r=0 \\ (k_f, k_s) \in \mathcal{M}}}^R \epsilon^r \mathbf{b}(\mathcal{Y}^{(R)}, Y_s^{(R)}) e^{i(k_f \phi_f^{(R)} + k_s \phi_s^{(R)})}. \quad (26)$$

If we replace the book-keeping parameter ϵ for its value equal to 1, we recover the final normal form, depending on the actions and the angles through the combination,

$$H_b^{(R)} = \sum_{(k_f, k_s) \in \mathcal{M}} \mathbf{c}_{(d_f, d_s, k_f, k_s)} \sqrt{\mathcal{Y}^{(R)}}^{d_f} \sqrt{Y_s^{(R)}}^{d_s} e^{i(k_f \phi_f^{(R)} + k_s \phi_s^{(R)})}, \quad (27)$$

where the pairs (d_f, k_f) and (d_s, k_s) have the same parity, and the values of the Fourier wavenumbers are bounded by $|k_f| \leq d_f$ and $|k_s| \leq d_s$. The integers (d_f, d_s) are limited by the value of R , through the book-keeping Rule 3.1.

We define the quantity

$$\Psi = m_1 \mathcal{Y}^{(R)} + m_2 Y_s^{(R)} \quad (28)$$

as a *resonant integral* of the normal form $H_b^{(R)}$, where m_1 and m_2 are the integers that define the resonant module \mathcal{M} in Eq. (17). Considering Eq. (16), it is straightforward to prove that

$$\mathcal{L}_{H_b^{(R)}} \Psi = \{H_b^{(R)}, \Psi\} = 0, \quad (29)$$

i.e. Ψ is a formal integral of $H_b^{(R)}$.

By considering the transformation $\mathcal{C}^{(R)}$,

$$\mathcal{C}^{(R)} = \varphi^{(1)} \circ \varphi^{(2)} \circ \dots \circ \varphi^{(R-1)} \circ \varphi^{(R)}, \quad (30)$$

where

$$\varphi^{(r)} = \exp(\mathcal{L}_{\chi_r}) (\mathcal{Y}^{(r)}, Y_s^{(r)}, \phi_f^{(r)}, \phi_s^{(r)}) \quad (31)$$

we can represent the resonant integral in terms of the original variables $(\mathcal{Y}^{(0)}, Y_s^{(0)}, \phi_f^{(0)}, \phi_s^{(0)})$, via

$$\Psi(\mathcal{Y}^{(0)}, Y_s^{(0)}, \phi_f^{(0)}, \phi_s^{(0)}) = \Psi\left(\mathcal{C}^{(R)}(\mathcal{Y}^{(R)}, Y_s^{(R)}, \phi_f^{(R)}, \phi_s^{(R)})\right). \quad (32)$$

Finally, applying the inverse transformations to those of Eqs. (14) and (12), we are able to express the resonant integral in (32) as function of the variables used in Eq. (11)

$$\Psi \equiv \Psi(v, \mathcal{Y}, u, \phi_f). \quad (33)$$

Having arrived at a final expression for the resonant integral Ψ in terms of the original canonical variables, we can compute the form of the theoretical separatrices of the corresponding secondary resonance in any suitably defined surface of section of the Hamiltonian H_b . In the numerical results below, we adopt a section of the form $\phi_f = \phi_{f0}$, as well as a constant value of the energy $E = H_b$, the equation $E = H_b(v, \mathcal{Y}, u, \phi_{f0})$ can be solved for \mathcal{Y} . Substitution to (33) yields then the resonant integral on the surface of section as a function of u and v only, viz.

$$\Psi \equiv \Psi\left(v, \mathcal{Y}(u, v; E, \phi_{f0}), u, \phi_{f0}\right). \quad (34)$$

The theoretical phase portrait is now obtained by the level curves of Eq. (34). Figure 2, left panel, summarizes the main features of the theoretical phase portrait. In particular, the stable periodic orbit of the secondary resonance is represented by the points of extremum of the level set of Ψ , while the unstable periodic orbit corresponds to the minimax (saddle) points of the level set of Ψ . The level curves with $\Psi = \Psi_{nmx}$, where Ψ_{nmx} is the value of the resonant integral at the saddle points, are the curves representing the theoretical separatrices of the secondary resonance.

4 Numerical results: boundary of the effective stability domain

4.1 Analytical vs. numerical stability boundary

We present below numerical results based on the computation of stability maps for selected values of the parameters μ and e' , characterized by the presence of conspicuous secondary resonances of the Hamiltonian H_b . The stability maps are given in color scale of the values of the Fast Lyapunov Indicator ([14]), for orbits with initial conditions labeled in terms of two quantities $(\Delta u, e_{p_0})$. These quantities also serve as proper elements, i.e. quasi integrals of motion, for the subset of all regular orbits in every stability map. Working on fixed surfaces of section $\phi_f = -\pi/3$, the relation between initial conditions (u, v, \mathcal{Y}) and $(\Delta u, e_{p_0})$ is given by the relations $\mathcal{Y} = \frac{e_{p_0}^2}{2}$, $\Delta u = u - u_0$, where u_0 is the point of intersection of the short-period orbit around L4 with the surface of section (see [33] for analytical expressions), and $v = B\Delta u$, for fixed parameters B (depending on μ) selected in such a way that the straight line $v = B(u - u_0)$ in the surface of section passes right through one of the islands of the secondary resonance chain. The half-width of the libration in u as a function of Δu , B , μ , e_p and e' , reads

$$D_p = \left[\frac{3B^2/2 + \mu(9/8 + 63e'^2/16 + 129e_p^2/64)}{\mu(9/8 + 63e'^2/16 + 129e_p^2/64)} \right]^{1/2} \Delta u + \mathcal{O}(\Delta u^2). \quad (35)$$

The values of B used in the various stability maps below are given explicitly in the caption of each figure.

We can now superpose the theoretical computation of the phase portrait of the secondary resonance to the numerical results found in the stability maps. For given parameters μ , e' , B , and choosing one value of the energy E , one obtains the resonant integral (34) as a function of u only. An example is shown in the right panel of Fig. 2. The value $u = \bar{u}$ marks the position of local maximum of the resonant integral Ψ along the line $v = B(u - u_0)$. This corresponds a central locus passing approximately through the middle of the resonant domain along the corresponding secondary resonance.

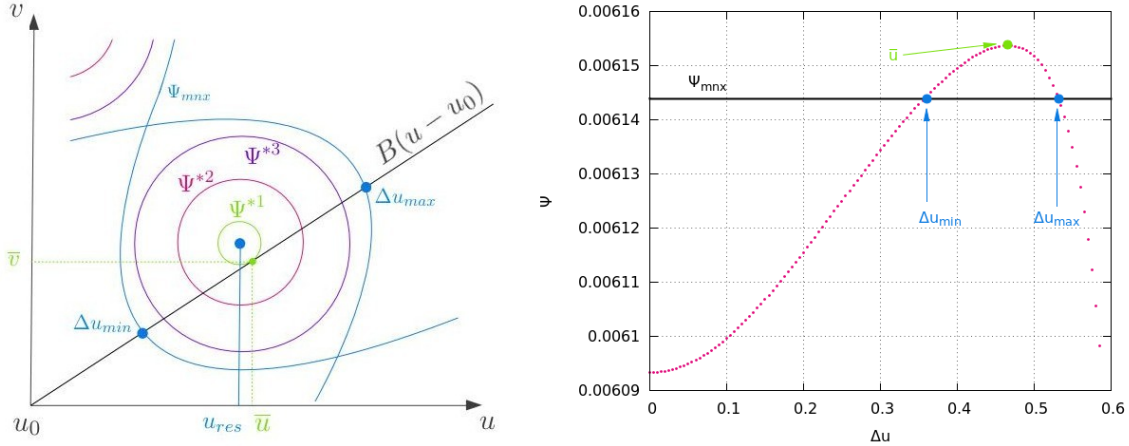


Figure 2: Left panel - Schematic representation of the plane (u, v) for a surface of section of the H_b . The central blue dot represents the location of a stable periodic orbit, whose co-ordinate in equal to $u = u_{res}$. At this point, the resonant integral Ψ presents a global extremum. Additional quasi-periodic orbits inside the island of stability are labeled with the corresponding values of Ψ , i.e. Ψ^{*1} , Ψ^{*2} , Ψ^{*3} , Ψ_{mnx} , accomplishing $\Psi^{*1} > \Psi^{*2} > \Psi^{*3} > \Psi_{mnx}$. The value Ψ_{mnx} represents a theoretical separatrix of the resonance in the resonant integral approximation (in reality, instead of the separatrix we have a thin separatrix-like chaotic layer). For the initial conditions taken along the line $B(u - u_0)$, the orbit for which Ψ is maximum corresponds to a level curve tangent to the line, labeled Ψ^{*1} . The initial condition for u along this line, \bar{u} , represents a good approximation to the exact resonant position u_{res} . The two values of u on the line $B(u - u_0)$ satisfying $\Psi = \Psi_{mnx}$ correspond to the intersection of the separatrix with the line $B(u - u_0)$ (Δu_{min} and Δu_{max} , in blue), and provide an estimation of the width of the resonance. Right panel - Values of the resonant integral Ψ along the line $B(u - u_0)$. The position of the maximum of the function corresponds to \bar{u} (green dot). The value of Ψ_{mnx} (black line) defines the position of the two borders of the resonance Δu_{min} and Δu_{max} (blue dots).

On the other hand, the points of intersection of the line $\Psi = \Psi_{mnx}$ with the curve of the resonant integral mark the values u_1, u_2 , and hence $\Delta u_{min} = u_1 - u_0$, $\Delta u_{max} = u_2 - u_0$, where the theoretical separatrix intersects the plane of the stability map. The corresponding values of e_{p0} can be found through $e_{p0,i} = \left[-2\mathcal{Y}(u_i, v_i = B(u_i - u_0), \phi_{f0}; E) \right]^{1/2}$, with $i = 1, 2$.

Repeating, now, the same process for different values of the energy E allows to obtain the whole locus of the theoretical center as well as the theoretical boundary of the secondary resonance on the FLI stability map. Figure 3 shows an example of the location of the center and borders of a secondary resonance, with the method of the resonant integral, for the case of the 1:6 secondary resonance ($\mu = 0.0041$) and $e' = 0.02$. The position of the center of the resonance is denoted by a dashed line, and the inner and outer borders are denoted by thick solid lines. By comparison with the underlying FLI stability map, we can see that both the center of the resonance and the outer border Δu_{max} are underestimated by this computation, proving that the overall estimation of the resonance width is not accurate. On the other hand, the key remark is that the method turns to be extremely efficient in the location of the inner border. The approximate position of Δu_{min} is well determined in the whole range of proper eccentricity values considered $0 < e_{p,0} < 0.1$.

Figure 4 shows more examples of the method of determination of the effective stability domain through the application of the resonant normal form in the cases of the secondary resonances 1:5 ($\mu = 0.0056$, panel a), 1:6 ($\mu = 0.0041$, panel b), 1:7 ($\mu = 0.0031$, panel b) and 1:8 ($\mu = 0.0024$, panel d), and primary's eccentricity $e' = 0.02$. In all the panels, the location of the inner border Δu_{min} is

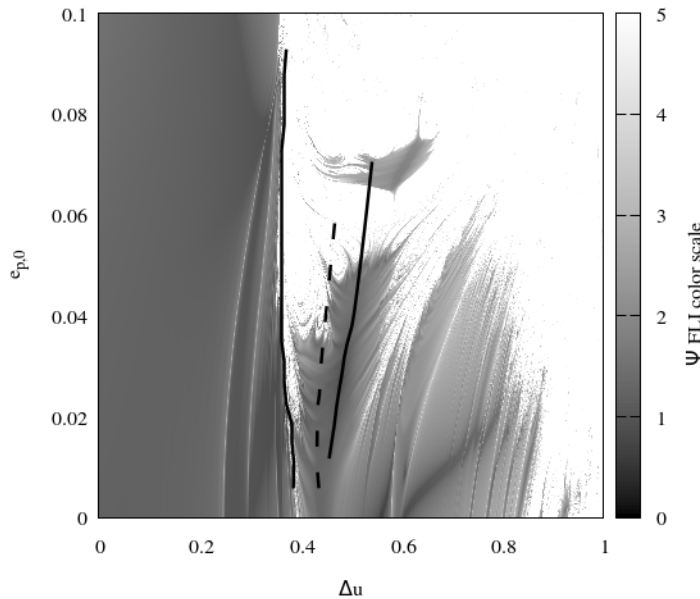


Figure 3: Theoretical location of the center and borders of the 1:6 secondary resonance for $\mu = 0.0041$, $B = 0$ and $e' = 0.02$. The solid lines correspond to the inner and outer border of the resonance, the dashed line corresponds to the estimation of the center of the resonance. The underlying image gives the numerical stability map, using the FLI value in grayscale.

shown with a thick black line on top of the corresponding FLI stability map. We observe that this limit divides the space of proper elements in two regions: the inner domain from $\Delta u = 0$ to Δu_{min} is populated mainly by regular orbits, and exhibits also some isolated resonances of small width, in which the orbits can only be weakly chaotic and remain practically stable. On the contrary, the domain external to Δu_{min} is dominated by the presence of conspicuous resonances as well as regions of strong chaos. It is remarkable that the analytical determination of the inner border of the resonances, which is based on an integrable approximation to the Hamiltonian (i.e. the resonant normal form), can still provide an accurate limit even in domains of the phase space where the resonant orbits are, in reality, chaotic. It is this robustness of the inner border determination which renders the whole approach useful in practice.

Figures 5 and 6 show, now, more examples of the applicability as well as the level of approximation of the method. Figure 5 shows the stability maps for $\mu = 0.0041$ (corresponding to a conspicuous 1:6 secondary resonance) and three different values of the primary's eccentricity, $e' = 0.02$ (panel a), $e' = 0.06$ (panel b), $e' = 0.1$ (panel c). In the same plots we show the effective stability borders from the resonant normal form computation for the 1:6 secondary resonance, but for two values of the primary's eccentricity in each case, namely $e' = 0$ (dotted thin line) and $e' = 0.02$ (thick line) in (a), $e' = 0$ (dotted thin line) and $e' = 0.06$ (thick line) in (b) and $e' = 0$ (dotted thin line) and $e' = 0.1$ (thick line) in (c). We observe that altering the primary's eccentricity from $e' = 0$ to only $e' = 0.1$ suffices to completely wipe out the entire structure of secondary resonances beyond $\Delta u \simeq 0.4$. In fact, we observe that, with increasing e' , so called 'transverse' resonances, i.e. involving also the secular frequency g , i.e. of the form $m_f \omega_f + m_s \omega_s + m_g g = 0$ with $m_g \neq 0$, appear near this border. For example, the 1:6:1 resonance at $u \sim 0.25$ in panel (a) of Fig. 5 moves towards the border at $u \approx 0.35$ in panel C of the same figure. A careful inspection of the stability maps shows that, for small e' these resonances have a small width and remain isolated within the inner stability domain, while, as e' increases, all resonances (main or transverse) grow in size and move outwards, until they enter to the region of strong chaos. As revealed in the panels of Fig. 5, these two effects (the moving of the resonances outwards and the refilling of the stable region with transverse resonances) counteract each other in such a way that the border separating the inner domain of stability from the outer chaotic

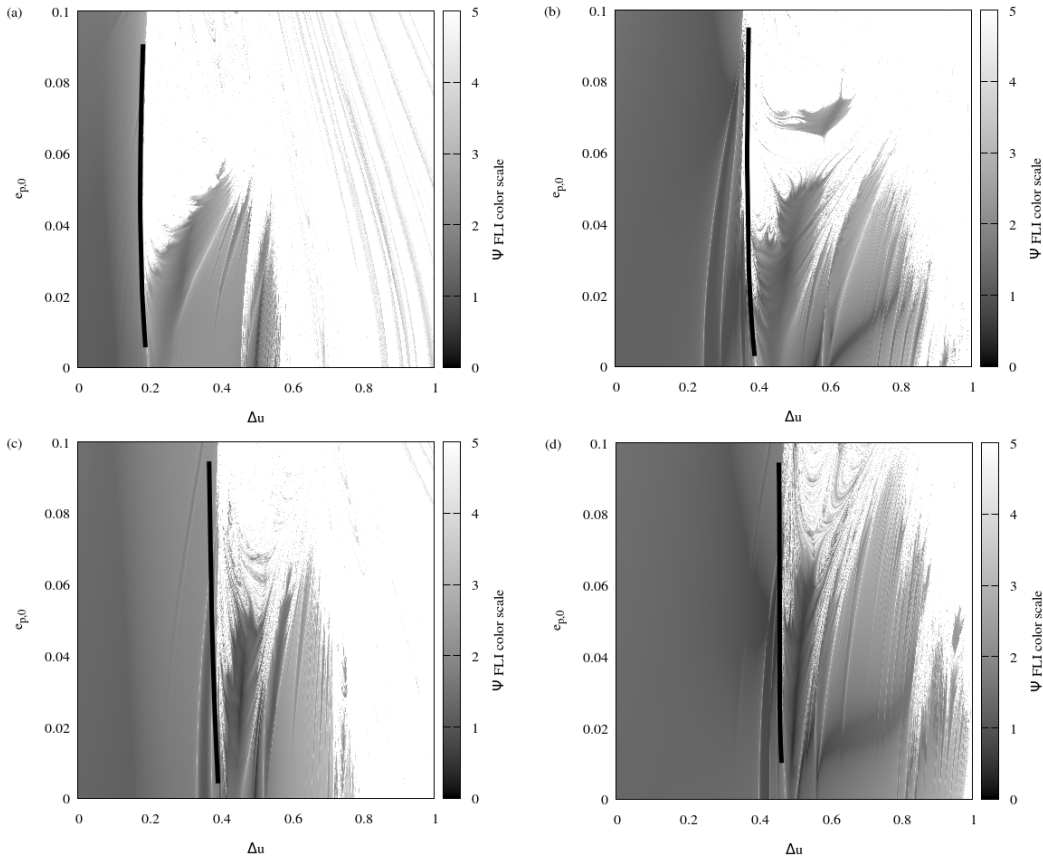


Figure 4: Determination of the effective stability domain (Δu_{min} , thick black line), for the secondary resonances 1:5 ($\mu = 0.0056$, $B = 0.03$, panel a), 1:6 ($\mu = 0.0041$, $B = 0$, panel b), 1:7 ($\mu = 0.0031$, $B = 0.015$, panel c) and 1:8 ($\mu = 0.0024$, $B = 0$, panel d), and $e' = 0.02$.

domain remains practically in the same place. Due to this effect, we can see that even the estimation of the border via the resonant normal form corresponding to the *circular* case ($e' = 0$, dotted thin line) practically suffices to obtain a good approximation of the border of the effective stability domain. Also, regarding the Trojan's body eccentricity, parameterized by $e_{p,0}$, one remarks that stable domains of all the secondary resonances, beyond the main stability domain, survive only for small values of $e_{p,0}$. This is because the amplitude of the separatrix pulsation increases as the eccentricity of the Trojan body increases. As a consequence, we find that the border of the main domain of stability is more sharp, and, thus, in general, better represented by the analytical resonance limit as $e_{p,0}$ increases.

Similar results are found in Fig. 6, showing the stability maps for $\mu = 0.0056$, corresponding to a conspicuous 1:5 secondary resonance, and for the primary's eccentricity values $e' = 0.02$ (panel a), $e' = 0.08$ (panel b). The estimated borders are found by the resonant normal form determination for $\mu = 0.0056$, using the parameters $e' = 0$ (circular case, dotted thin line) and $e' = 0.02$ (thick line) in (a), and $e' = 0$ (dotted thin line) and $e = 0.08$ (thick line) in (b). The margin between the two theoretical curves is again small (of about 0.02 rad in Δu), while, again, the determination of the border of the stability domain using the circular model suffices to practically obtain an accurate limit of the domain of stability. In fact, in both Figures 5 and 6 the extent occupied by the stable parts of the corresponding resonances is determined by the separatrix pulsation effect. The amplitude of the pulsation depends on terms absent from the 'basic model', thus this effect cannot be modelled using only the resonant integrals of the basic model. However, as a rule of thumb we find that the border of the domain of stability lies always between two theoretical border determinations by the basic model, i.e., one using the circular model $e' = 0$ and a second using a moderate value of the

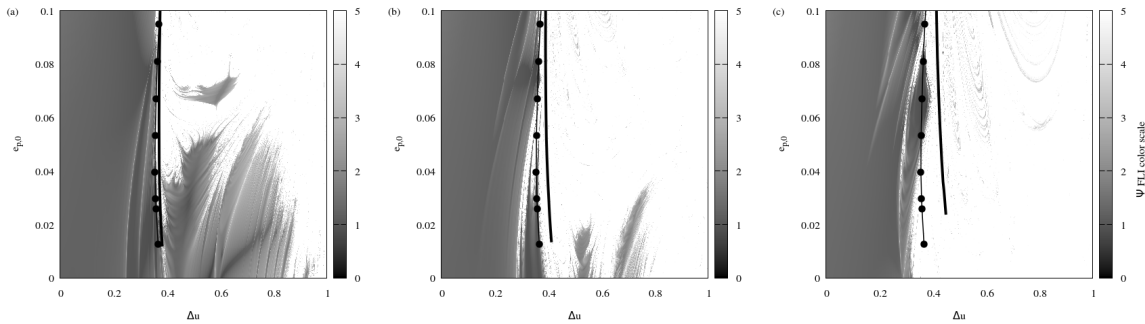


Figure 5: FLI stability maps for the 1:6 secondary resonance ($\mu = 0.0041$, $B = 0$) and three values of the eccentricity $e' = 0.02$ (a), $e' = 0.06$ (b), $e' = 0.1$ (c). The dotted thin line corresponds to the analytical determination of Δu_{min} for the parameters $\mu = 0.0041$ and $e' = 0$ (circular case) in all three panels, while the thick line corresponds to $e' = 0.02$ in (a), $e' = 0.06$ in (b) and $e' = 0.1$ in (c).

primary's eccentricity, e.g. $e' = 0.1$.

4.2 Robustness with respect to parameter values

The investigation in the previous subsection focused on particular values of μ selected with the criterion that, for low eccentricities of either the primary perturber or the test body ($e', e_{p,0} < 0.1$), the phase space of the basic model is dominated by a low-order secondary resonance of the form 1: n with $n = 5, 6, \dots$. Repeating a comparison between FLI maps and innermost separatrix borders of secondary resonances, a behavior similar to Figures 6 (resonance 1:5, for $\mu = 0.0056$) and 5 (resonance 1:6, for $\mu = 0.0041$) for low eccentricities is found when one considers the resonances 1:7 for $\mu = 0.0031$, 1:8 for $\mu = 0.0024$, 1:9 for $\mu = 0.0021$, 1:10 for $\mu = 0.0016$, 1:11 for $\mu = 0.0014$, 1:12 for $\mu = 0.0012$. These values of μ are shifted positively with respect to the bifurcation values $\mu = \mu_{1:n}$ of each corresponding 1: n short period family in the basic model. The shift reflects the fact that, keeping $e', e_{p,0}$ constant, and increasing μ as $\mu = \mu_{1:n} + \Delta\mu$, with $\Delta\mu > 0$, the resonance 1: n moves outwards from the libration center, i.e., towards higher libration amplitudes Δu , as $\Delta\mu$ increases. In the resonant integral approximation, the outward motion of each resonance is accompanied by an increase of its separatrix width. However, the integrable approximation fails due to resonance overlap with nearby resonances as $\Delta\mu$ increases. This antagonism between outward expansion and resonance overlap determines the real limit of the domain of stability (see [40], [6] for a description of this phenomenon in simple dynamical maps).

The bifurcation value $\mu_{m:n}$ for the $m:n$ short-period family of the basic model can be estimated by the root for μ of the equation:

$$m(1 - 27\mu/8) = n\sqrt{6\mu\left(\frac{9}{8} + \frac{63e'^2}{16} + \frac{129e_p^2}{64}\right)} \quad (36)$$

Applying Eq. (36) to the 1:6 resonance, we find $\mu_{1:6} \approx 0.0040$ for $e' = e_p = 0.02$, while $\mu_{1:6} \approx 0.0038$ for $e' = e_p = 0.1$. As evident from Fig. 5, the resonance is clearly dominant at $\mu = 0.0042$. In fact, we find that the 1:6 resonant integral inner separatrix limit applies already when $\Delta\mu \geq 0.001$ with respect to the bifurcation value for low eccentricities. On the other hand, as shown in panels (a) and (e) of Fig. 7, the analytical series computation with the 1:6 resonant integral starts collapsing when $\mu = 0.0044$, or $\Delta\mu \approx 0.004$. In practice, the whole separatrix domain around the 1:6 resonance has been transformed into a chaotic domain. Thus, while it remains true that the 1:6 resonance of the basic model delimits the main stability domain, the convergence of the series representing the theoretical computation of the corresponding resonant integral becomes poor.

Implementing, now, Eq. (36) to the 1:5 resonance we find $\mu_{1:5} \approx 0.0057$ for $e' = e_{p,0} = 0.02$, while $\mu_{1:5} \approx 0.0054$ for $e' = e_{p,0} = 0.1$. Thus $\mu_{1:5} - \mu_{1:6} \approx 0.0016$, which implies that the distance in μ

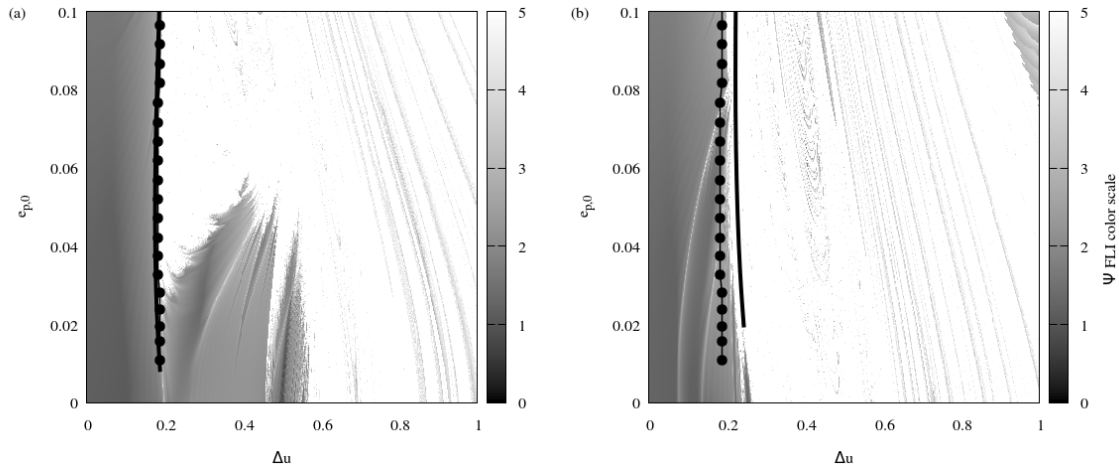


Figure 6: FLI stability maps for the 1:5 secondary resonance ($\mu = 0.0056$, $B = 0.03$) and two values of the eccentricity $e' = 0.02$ (a), $e' = 0.08$ (b). The dotted thin line corresponds to the analytical determination of Δu_{min} for the parameters $\mu = 0.0056$ and $e' = 0$ (circular case) in the two panels, while the thick line corresponds to $e' = 0.02$ in (a) and $e' = 0.08$ in (b).

separating the resonances 1:6 and 1:5 is about 3-4 times larger than the interval of values of $\Delta\mu$ for which the validity of the resonant integral computation using one particular resonance is satisfactory. In principle, in order to bridge the gap between the two resonances, one has to use higher order resonances of the basic model, since the border of the domain of stability is always delimited by one such resonance. In practice, we find that it suffices to consider the basic resonances $1:n$ and their first Farey tree combination, i.e., the resonances $2:(2n-1)$ which bifurcate at intermediate values of μ , i.e. $\mu_{1:n} < \mu_{2:2n-1} < \mu_{1:n-1}$ for fixed e', e_p . Figure 7 exemplifies the transition from the dominance of the 1:6 to the 1:5 resonance via the 2:11 resonance of the basic model, for two values of the primary's eccentricity $e' = 0.02$ (upper row) and $e' = 0.08$ (lower row). The collapse of the inner border calculation for the 1:6 resonances starts near $\mu = 0.0044$. However, the computation using the 2:11 resonant integral restores a correct estimate of the main domain of stability for $\mu = 0.0048$, leaving only secondary resonances outside this domain. The 2:11 resonance remains dominant in this respect up to $\approx \mu = 0.0054$. At this value of μ the 1:5 secondary resonance of the basic model bifurcates for large enough values of the eccentricities, a fact which implies that the whole domain beyond the innermost separatrix of the 1:5 resonance should now be considered as outside the main stability domain. Indeed, although these secondary resonances are still very stable for very low eccentricities, we see that they essentially disappear for values of the eccentricities near ≈ 0.1 (compare panels (d) and (i) of Fig. 7). This marks the transition from the dominance of the 2:11 to the 1:5 resonance, the latter one being clearly dominant for a somewhat still higher value of μ ($\mu = 0.0056$ in panels e, j).

Figure 8 shows in greater detail the transition from the 2:11 to the 1:5 resonance, which, using FLI stability maps of the full problem, is actually seen to involve also some resonances coined *transverse* in [33], i.e. resonances involving all three short, synodic and secular frequencies. In particular, we see that the border of stability, which for $\mu = 0.0049$ is practically delimited by the 2:11 resonance, starts being gradually penetrated by the transverse resonances 2:11:1, 1:5:2 and 1:5:1. The penetration appears earlier, as μ increases, for higher values of the eccentricities. This effect leaves small windows of values of μ for which, for low eccentricities, the border of stability may appear dominated by the innermost separatrix of some transverse resonance (e.g. the resonance 1:5:1 in panel (c) for $\mu = 0.0053$, $e' = 0.02$). However, for the same value of μ , the innermost separatrix border of the 1:5 resonance appears also in the upper part of the stability map for higher primary's eccentricity, i.e., $e' = 0.08$ (panel g). As a consequence, although a clear dominance of the 1:5 resonance occurs for all eccentricities beyond $\mu = 0.0055$ (panels d, h), the 1:5 resonance practically dominates in a

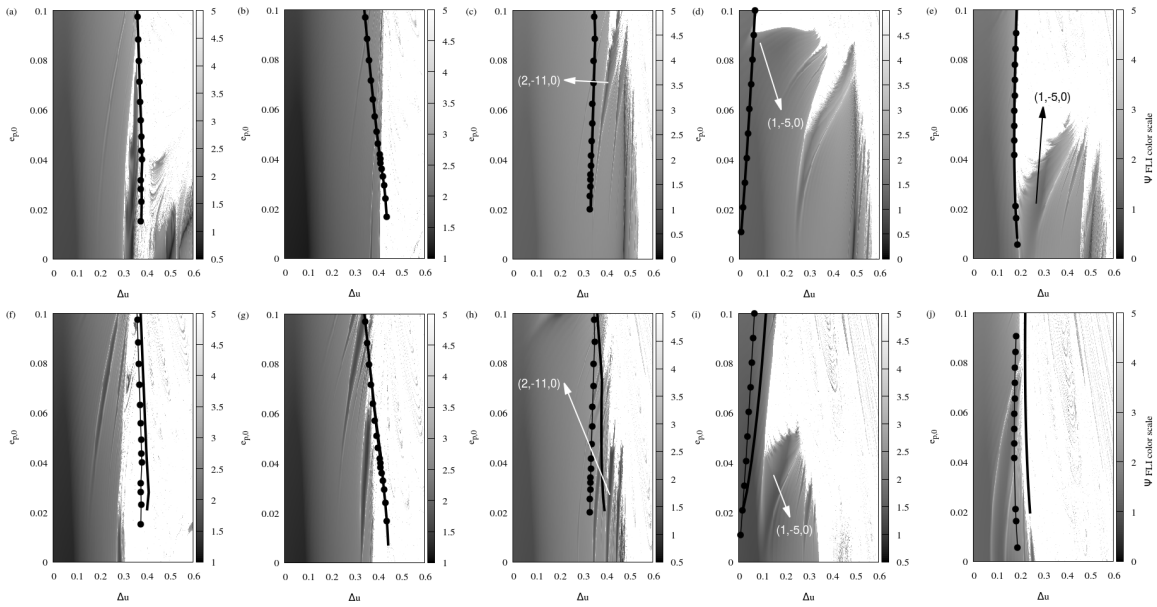


Figure 7: FLI stability maps for $\mu = 0.0042$ and $e' = 0.02$ (a), $\mu = 0.0044$ and $e' = 0.02$ (b), $\mu = 0.0048$ and $e' = 0.02$ (c), $\mu = 0.0054$ and $e' = 0.02$ (d), $\mu = 0.0056$ and $e' = 0.02$ (e), $\mu = 0.0042$ and $e' = 0.08$ (f), $\mu = 0.0044$ and $e' = 0.08$ (g), $\mu = 0.0048$ and $e' = 0.08$ (h), $\mu = 0.0054$ and $e' = 0.08$ (i), and $\mu = 0.0056$ and $e' = 0.08$ (j). The thick lines yield the analytical estimation of the border of stability for the corresponding value of μ and $e' = 0.02$ for the upper row panels, and $e' = 0.08$ for the lower row panels. The dotted thin line yields the analytical estimation of the border for the corresponding value of μ and $e' = 0$ (circular case) in all the panels. $B = 0.03$ for all the panels.

wide range of eccentricities already at $\mu = 0.0053$. In fact, this dominance can only become more pronounced when additional perturbations are added to the model.

In conclusion, except for small transient windows of parameter values, one can practically always find a resonance of the basic model for which the innermost separatrix provides the limit of the main domain of stability. It is to be stressed that this is a physical property induced by resonant dynamics, which holds independently of the efficiency by which the innermost separatrix border of the resonance can be computed analytically using some form of resonant integral series. On the other hand, using the method presented in Section 3.2, we find precise results by limiting the choice of resonance of the basic model among the set $1:n$ or $2:(2n-1)$, with n integer. As a rule of thumb, for given parameters μ, e' we choose the limiting resonance as the rational number closer to the frequency ratio:

$$f = \frac{\sqrt{6\mu \left(\frac{9}{8} + \frac{63e'^2}{16} + \frac{129e_p^2}{64} \right)}}{(1 - 27\mu/8)} \quad (37)$$

for values of e_p within our domain of interest.

4.3 Robustness with respect to the choice of model

As an additional test, we examine the robustness of the above results against changing the dynamical model for Trojan orbits. Several formation scenarios discussed in literature ([1], [3], [16], [25], [32]) have allowed relatively massive Trojan planets (of mass ~ 1 Earth mass) to exist. Allowing the Trojan body to have considerable mass, we examine whether the stability borders found in the framework of the ‘basic model’, which is only derived from the ERTBP, are still applicable in the framework of the full planar three body problem.

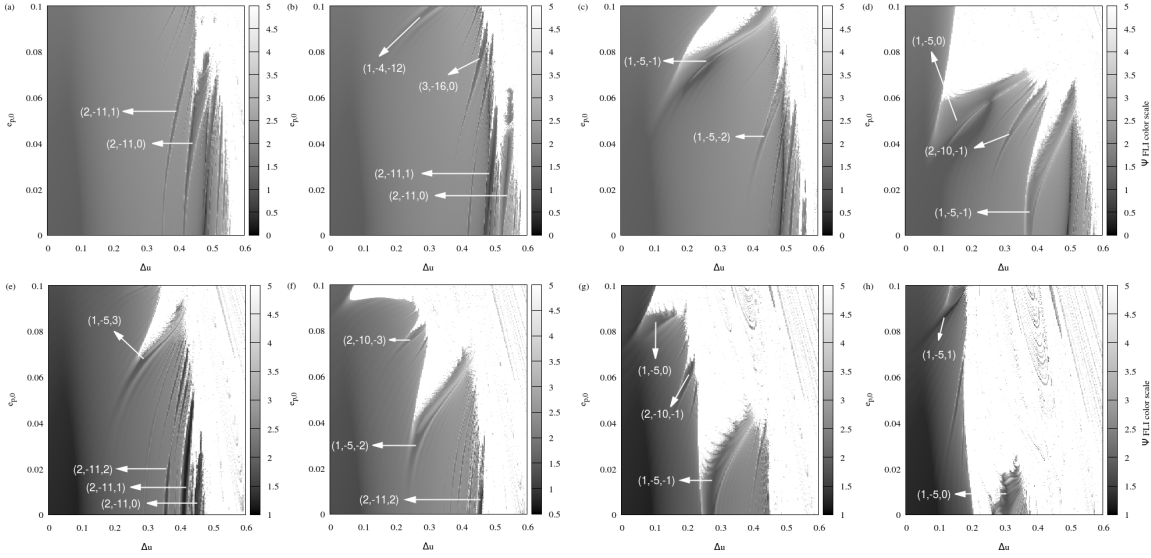


Figure 8: Details of the transition from the dominance of the 2:11 to the 1:5 resonance as μ varies from $\mu = 0.0049$ to $\mu = 0.0055$. The parameters in each panel are (a). $\mu = 0.0049$, $e' = 0.02$, (b). $\mu = 0.0051$, $e' = 0.02$, (c). $\mu = 0.0053$, $e' = 0.02$, (d). $\mu = 0.0055$, $e' = 0.02$, (e). $\mu = 0.0049$, $e' = 0.08$, (f). $\mu = 0.0051$, $e' = 0.08$, (g). $\mu = 0.0053$, $e' = 0.08$, H. $\mu = 0.0055$, $e' = 0.08$. The domains of various resonances (including transverse ones) are marked in the same plots.

As an example, Figure 9 compares the border of stability in the planar ERTBP for $\mu = 0.0041$ with one computed in the full three body problem with the Trojan body having mass equal to 1 or 10 Earth masses. We consider the Hamiltonian in Poincaré variables:

$$H = \frac{p_1^2}{2m_1} + \frac{p_2^2}{2m_2} + \frac{(p_1 + p_2)^2}{2m_0} - \frac{Gm_0m_1}{r_1} - \frac{Gm_0m_2}{r_2} - \frac{Gm_1m_2}{\Delta} \quad (38)$$

where m_0, m_1, m_2 are the masses of the star, perturbing primary and Trojan planet respectively, $\mathbf{r}_1, \mathbf{r}_2$ the heliocentric positions of the primary and Trojan planet, $\Delta = \mathbf{r}_1 - \mathbf{r}_2$ and $\mathbf{p}_1, \mathbf{p}_2$ their corresponding barycentric momenta. In order to use same units as in the ERTBP, one notes that the equations of motion in Cartesian heliocentric co-ordinates $\mathbf{r}_1 \equiv (r_{1x}, r_{1y})$, $\mathbf{r}_2 \equiv (r_{2x}, r_{2y})$, and barycentric velocities $\mathbf{p}_1/m_1 \equiv (v_{1x}, v_{1y})$, $\mathbf{p}_2/m_2 \equiv (v_{2x}, v_{2y})$ only depend on the variables $r_{ix}, r_{iy}, v_{ix}, v_{iy}$, $i = 1, 2$ and on the constants Gm_0, Gm_1, Gm_2 . Then, we solve $Gm_0 + Gm_1 = 1$, $Gm_1 = \mu$ and assign a value to $Gm_2 = Gm_0(m_2/m_0)$ according to the considered mass ratio $\mu_2 = m_2/m_0$.

In order now to obtain comparable FLI maps in the two problems, we proceed as follows. For every point on the plane of the stability map of the ERTBP (such as in Fig. 9a), we compute the corresponding heliocentric positions and velocities of both the primary and the Trojan, i.e. $(r_{ix}(t=0), r_{iy}(t=0), \dot{r}_{ix}(t=0)$ and $\dot{r}_{iy}(t=0)$, with $i = 1, 2$. From Hamilton's equations of (38) one readily sees that the barycentric velocities (v_{ix}, v_{iy}) , $i = 1, 2$ of both bodies are linear functions of the heliocentric ones. Thus, from every point of the FLI map in the ERTBP, we compute the complete set of corresponding initial conditions $r_{ix}(t=0), r_{iy}(t=0), v_{ix}(t=0)$ and $v_{iy}(t=0)$ needed in order to integrate the full Three Body problem. Via the same process we assign also corresponding initial conditions for the variational equations of motion in the two problems.

Figure 9 shows the comparison of the FLI stability maps in the case of dominance of the 1:6 resonance, at $\mu = 0.0041$ as μ_2 evolves, i.e., $\mu_2 = 3 \times 10^{-6}$ (1 Earth mass, upper row), or $\mu_2 = 3 \times 10^{-5}$ (10 Earth masses, lower row). The left, middle and right panels correspond to initial eccentricities of the primary equal to $e' = 0.02$, $e' = 0.06$ and $e' = 0.1$. Thus, these maps are comparable with the ones under the ERTBP (Fig. 5). The main observation is that switching on the mass m_2 results in a considerable reduction of the area occupied by the stable domains of the secondary resonances.

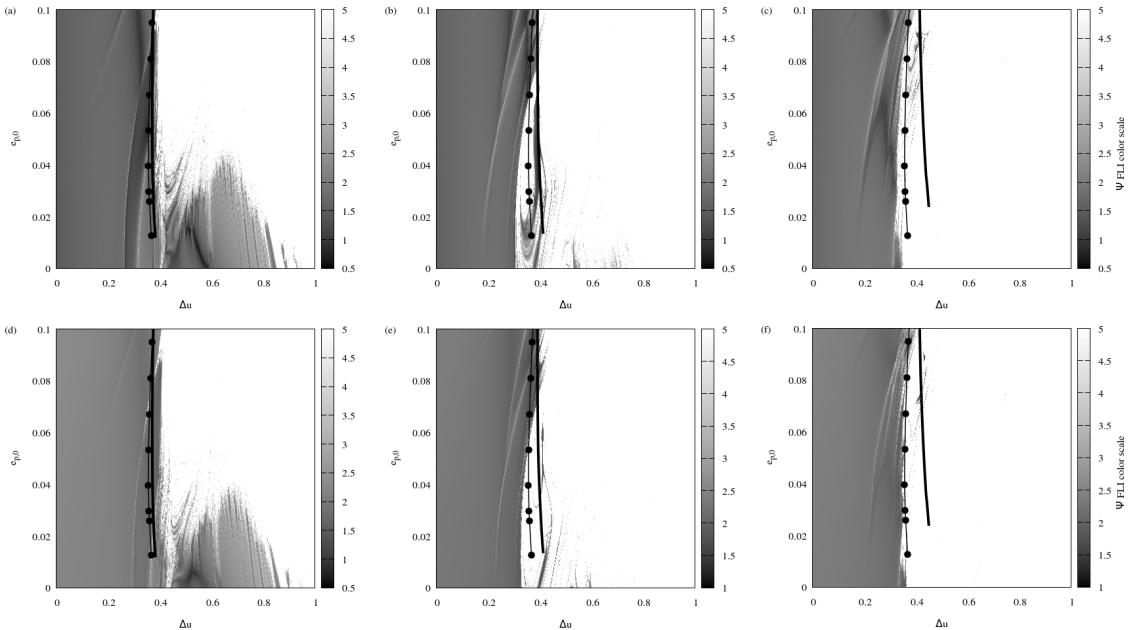


Figure 9: The FLI stability maps obtained with the same initial conditions as in Fig.5, but running the full planar three body model instead of the ERTBP, with a mass $\mu_2 \neq 0$ assigned to the Trojan body. The mass of the primary is always $\mu = 0.0041$, while the remaining parameters (initial eccentricity e' of the primary and mass μ_2 of the Trojan) are (a). $e' = 0.02$, $\mu_2 = 3 \times 10^{-6}$, (b). $e' = 0.06$, $\mu_2 = 3 \times 10^{-6}$, (c). $e' = 0.1$, $\mu_2 = 3 \times 10^{-6}$, (d). $e' = 0.02$, $\mu_2 = 3 \times 10^{-5}$, (e). $e' = 0.06$, $\mu_2 = 3 \times 10^{-5}$, (f). $e' = 0.1$, $\mu_2 = 3 \times 10^{-5}$. The analytical curves are those of Fig. 5.

This is mostly caused by the secular variations induced on the orbit of the primary planet, which increase the amplitude of modulation of the separatrices of each secondary resonance. However, the main domain of stability remains nearly unaffected by these phenomena, and retains a quite similar width in all simulations with different masses μ_2 . We only see some transverse resonances penetrating the lowermost (with respect to the eccentricities) part of the stability map for μ_2 as large as 10 Earth masses. On the other hand, the analytical determination of the innermost separatrix via the resonant integral of the ‘basic model’ yields an estimate of the border of the main stability domain which remains robust against the increase of μ_2 .

5 Conclusions

In the present work, we discussed a new application for the ‘basic Hamiltonian model’ H_b for Trojan motions presented originally in [33]: this is the determination of the border of effective stability, using the theoretical separatrices of the most conspicuous secondary resonances of H_b . In detail:

1) We compute resonant normal forms for various secondary resonances of H_b , using an ‘asymmetric expansion’ for the Hamiltonian (see Section 2), which allows to speed up the convergence of both the original polynomial representation of the Hamiltonian as well as its normal form. The improvement obtained by the asymmetric expansion is demonstrated with numerical examples.

2) Using the classical normal form construction with Lie series in order to compute a resonant normal form for a specific secondary resonance, one ends with an expression for an invariant of the normal form called the ‘resonant integral’ Ψ (see Section 3). The level curves of Ψ allow, in turn, to obtain a theoretical phase portrait on a surface of section, and in particular to compute theoretical separatrices as well as the center of the secondary resonance.

3) The method typically yields underestimates of the position of the center and outer separatrix of

the resonance, but a very efficient determination of the inner (closer to the libration center) separatrix of the resonance.

4) We argued that the inner limit $\Delta u_{min}(e_{p,0})$ found in this way represents a clear border which exists in numerical stability maps between two well distinct domains in the space of the proper elements $(\Delta u, e_{p,0})$ (see Section 4 for definitions). The inner domain is populated by regular orbits and isolated resonances with regular or marginally chaotic orbits, while the outer domain hosts either closely packed secondary resonances or a strongly chaotic domain. In fact, with increasing value of the primary's eccentricity e' , a modulation mechanism essentially wipes out all the resonances, creating a large outer domain of strong chaos. As a consequence, we argued that the inner domain, delimited by the innermost theoretical separatrix of the most conspicuous secondary resonance of H_b practically coincides with the limit of the effective stability domain for Trojan motions.

5) We demonstrated that the role of the secondary resonances of the basic model H_b , as delimiters of the domain of effective stability, covers most of the values of the parameters entering the problem (primary's mass and eccentricity, Trojan body's eccentricity), while it remains robust even in the full Three Body problem, for Trojan bodies of mass ~ 1 Earth mass.

Acknowledgements: Useful discussions with Prof. U. Locatelli are gratefully acknowledged. R.I.P. was supported by the Research Committee of the Academy of Athens, under the grant 200/854.

Appendix A

The variables corresponding to the three degrees of freedom appearing in the expression of the basic Hamiltonian H_b in Eq.(5), (u, v) , (Y_f, ϕ_f) and (Y_p, ϕ_p) are given in terms of the orbital elements as follows:

$$u = \lambda - \lambda' - \frac{\pi}{3} \quad , \quad (39)$$

$$v = \sqrt{a} - 1 \quad , \quad (40)$$

$$\beta = \omega - \phi' \quad ,$$

$$y = \sqrt{a} \left(\sqrt{1 - e^2} - 1 \right) \quad ,$$

$$V = \sqrt{-2y} \sin \beta - \sqrt{-2y_0} \sin \beta_0 \quad ,$$

$$W = \sqrt{-2y} \cos \beta - \sqrt{-2y_0} \cos \beta_0 \quad ,$$

$$Y = - \left(\frac{W^2 + V^2}{2} \right)$$

$$\phi = \arctan \left(\frac{V}{W} \right) \quad (41)$$

$$\phi_f = \lambda' - \phi \quad , \quad (42)$$

$$Y_f = \int \frac{\partial E}{\partial \lambda'} dt + v \quad , \quad (43)$$

$$Y_p = Y - Y_f \quad , \quad (44)$$

where λ , ω , a and e are the mean longitude, the longitude of the perihelion, the major semiaxis and eccentricity of the Trojan body, λ' and $\phi' = \omega'$ are the mean longitude and longitude of the perihelion of the perturber, $\beta_0 = \pi/3$, $y_0 = \sqrt{1 - e'^2} - 1$, and E represents the total energy of the Trojan as computed from Eq. (1) (see [33] for further details in the construction).

Appendix B

The asymmetric expansion in terms of $u = \tau - \pi/3$, up to a generic order K for the functions $\frac{\cos \tau}{(2-2\cos \tau)^{N/2}}$, $\frac{\sin \tau}{(2-2\cos \tau)^{N/2}}$, $\cos^M \tau$ and $\sin^M \tau$, with $N, M \in \mathbb{N}$ fixed is given by

$$\frac{\cos \tau}{(2-2\cos \tau)^{N/2}} = \frac{1}{2^{N/2}} \sum_{k=0}^K \mathcal{M}_1(k) u^k + \mathcal{O}(u^K), \quad \text{where} \quad \mathcal{M}_1(k) = \sum_{i=k}^K \frac{1}{i!} F^{(i)}(\pi/2) \binom{i}{k} \left(-\frac{\pi}{6}\right)^{i-k},$$

$$\frac{\sin \tau}{(2-2\cos \tau)^{N/2}} = \frac{1}{2^{N/2}} \sum_{k=0}^K \mathcal{M}_2(k) u^k + \mathcal{O}(u^K), \quad \text{where} \quad \mathcal{M}_2(k) = \sum_{i=k}^K \frac{1}{i!} G^{(i)}(\pi/2) \binom{i}{k} \left(-\frac{\pi}{6}\right)^{i-k},$$

$$\cos^M \tau = \sum_{k=0}^K \mathcal{M}_3(k) u^k + \mathcal{O}(u^K), \quad \text{where} \quad \mathcal{M}_3(k) = \sum_{i=k}^K \frac{1}{i!} B_{M,M}^{(i)} \binom{i}{k} \left(-\frac{\pi}{6}\right)^{i-k},$$

$$\sin^M \tau = \sum_{k=0}^K \mathcal{M}_4(k) u^k + \mathcal{O}(u^K), \quad \text{where} \quad \mathcal{M}_4(k) = \sum_{i=k}^K \frac{1}{i!} C_{M,M}^{(i)} \binom{i}{k} \left(-\frac{\pi}{6}\right)^{i-k},$$

and

$$F^{(n)}(\pi/2) = \sum_{i=1}^{\lfloor \frac{n-1}{2} \rfloor} (n, 2i-1) (-1)^i f^{(n-(2i-1))}(\pi/2),$$

$$G^{(n)}(\pi/2) = \sum_{i=0}^{\lfloor \frac{n}{2} \rfloor} (n, 2i) (-1)^i f^{(n-2i)}(\pi/2),$$

with $\lfloor \frac{n-1}{2} \rfloor$ the integer part of $\frac{n-1}{2}$, and $\lfloor \frac{n}{2} \rfloor$ the integer part of $\frac{n}{2}$; the derivatives $f^{(n)}$ are given by

$$f^{(n)}(\pi/2) = \sum_{m=1}^n A_{m,m}^{(n)};$$

the coefficients $A_{m,m}^{(n)}$, $B_{M,M}^{(n)}$ and $C_{M,M}^{(n)}$ are given by

$$A_{m,m}^{(n)} = -A_{m,m-1}^{(n-1)} - \left(\frac{2(m-1) + N}{2} \right) A_{m-1,m-1}^{(n-1)}, \quad A_{1,1}^{(1)} = -\frac{N}{2},$$

$$B_{M,M}^{(n)} = -B_{M,M-1}^{(n-1)} + (M+1) B_{M,M+1}^{(n-1)}, \quad B_{1,1}^{(1)} = -M,$$

$$C_{M,M}^{(n)} = C_{M,M-1}^{(n-1)} - (M+1) C_{M,M+1}^{(n-1)}, \quad C_{1,1}^{(1)} = M.$$

For a proof of these formulæ, we refer the reader to [36].

References

- [1] Beaugé, C., Sándor, Z., Érdi, B., Süli, A., (2007) Co-orbital terrestrial planets in exoplanetary systems: a formation scenario, *Astron. Astrophys.* **463**, p 359.
- [2] Chirikov, B.V., Lieberman, M.A., Shepelyansky, D.L., Vivaldi, F.M., (1985) A theory of modulational diffusion, *Physica D* **12**, p 289.
- [3] Cresswell, P., Nelson, R.P., (2009) On the growth and stability of Trojan planets, *Astron. Astrophys.* **493**, p 1141.
- [4] Dobrovolskis, A., (2013) Effects of Trojan exoplanets on the reflex motions of their parent stars, *Icarus* **226**, p 1635.

- [5] Dvorak, R., Bazzó, A., Zhou, L.Y., (2010) Where are the Uranus Trojans?, *Celest. Mech. Dyn. Astron.* **107**, p 51.
- [6] Efthymiopoulos, C., Contopoulos, G., Voglis, N., (1999) Cantori, islands and asymptotic curves in the stickiness region *Celest. Mech. Dyn. Astron.* **73**, p 221.
- [7] Efthymiopoulos, C., Giorgilli, A., Contopoulos, G., (2004) Nonconvergence on formal integrals: II. Improved estimates for the optimal order of truncations *J. Phys. A* **37**, p 10831.
- [8] Efthymiopoulos, C. (2012) Canonical perturbation theory, stability and diffusion in Hamiltonian systems: applications in dynamical astronomy, in *Third La Plata International School on Astronomy and Geophysics: Chaos, diffusion and non-integrability in Hamiltonian Systems - Applications to Astronomy*, Cincotta, P.M., Giordano, C.M., Efthymiopoulos, C., eds, p 3.
- [9] Efthymiopoulos, C., (2013) High order normal form stability estimates for co-orbital motion, *Celest. Mech. Dyn. Astron.* **117**, p 101.
- [10] Érdi, B., (1988) Long periodic perturbations of Trojan asteroids, *Celest. Mech. Dyn. Astron.* **43**, p 303.
- [11] Érdi, B., (1997) The Trojan Problem, *Celest. Mech. Dyn. Astron.* **65**, p 149.
- [12] Érdi, B., Sandor, Z., (2005) Stability of co-orbital motion in exoplanetary systems, *Celest. Mech. Dyn. Astron.* **92**, p 113.
- [13] Érdi, B., Nagy, I., Sándor, Z., Süli, A., Fröhlich, G., (2007) Secondary resonances of co-orbital motions, *MNRAS* **381**, p 33.
- [14] Froeschlé, C., Guzzo, M., Lega, E., (2000) Graphical evolution of the Arnold web: from order to chaos, *Science* **289**, p 2108.
- [15] Giorgilli, A., Skokos, C., (1997) On the stability of the Trojan asteroids, *Astron. Astrophys.* **317**, p 254.
- [16] Giuppone, C., Benítez-Llambay, P., Beaugé, C., (2012) Origin and detectability of co-orbital planets from radial velocity data, *MNRAS* **421**, p 356.
- [17] Haghighipour, N., Capen, S., Hinse, T., (2013) Detection of Earth-mass and super-Earth Trojan planets using transit timing variation method, *Celest. Mech. Dyn. Astron.* **117**, p 75.
- [18] Laughlin, G., Chambers, J.E., (2002) Extrasolar Trojans: the viability and detectability of planets in the 1:1 Resonance, *Astron.J.* **124**, p 592.
- [19] Leleu, A., Robutel, P., Correia, A.C.M. (2015) Detectability of quasi-circular co-orbital planets. Application to the radial velocity technique, *Astron.Astrophys.* **581**, p A128
- [20] Leleu, A., (2016) Dynamics of co-orbital exoplanets - Ph.D. Thesis, *arXiv:1701.05585*
- [21] Leleu, A., Robutel, P., Correia, A.C.M., Lillo-Box, J. (2017) Detection of co-orbital planets by combining transit and radial-velocity measurements, *Astron.Astrophys.* **599**, p L7
- [22] Levison, H., Shoemaker, E., Shoemaker, C., (1997) Dynamical evolution of Jupiter's Trojan asteroids, *Nature* **385**, p 42.
- [23] Lhotka, C., Efthymiopoulos, C., Dvorak, R., (2008) Nekhoroshev stability at L_4 or L_5 in the elliptic restricted three-body problem—Application to Trojan asteroids, *MNRAS* **384**, p 1165.
- [24] Lykawka, P.S., Horner, J., Jones, B.W., Mukai, T., (2011) Origin and dynamical evolution of Neptune Trojans - II. Long term evolution, *MNRAS* **412**(1), p 537.
- [25] Lyra, W., Johansen, A., Klahr, H., Piskunov, N., (2009) Standing on the shoulders of giants: Trojan Earths and vortex trapping in low mass self-gravitating protoplanetary disks of gas and solids, *MNRAS* **493**, p 1125.
- [26] Marzari, F., Scholl, H., (2007) Dynamics of Jupiter Trojans during the 2:1 mean motion resonance crossing of Jupiter and Saturn, *MNRAS* **380**, p 479.

- [27] Milani, A., (1993) The Trojan asteroid belt: proper elements, stability, chaos and families, *Celest. Mech. Dyn. Astron.* **57**, p 59.
- [28] Morais, M.H.M, (1999) A secular theory for Trojan-type motion, *Astron. Astrophys.* **350**, p 318.
- [29] Morais, M.H.M, (2001) Hamiltonian formulation on the secular theory for a Trojan-type motion, *Astron. Astrophys.* **369**, p 677.
- [30] Nauenberg, M., (2002) Stability and eccentricity for two planets in a 1:1 resonances, and their possible occurrence in extrasolar planetary systems, *Astron. J.* **124**, p 2332.
- [31] Neishtadt, A.I., (1987) On the change in the adiabatic invariant on crossing a separatrix in systems with two degrees of freedom, *Prikl. Matem. Mekhan.* **51**(5), p. 750; *PMM USSR* **51**(5), p 586.
- [32] Pierens, A., Raymond, S.N., (2014) Disruption of co-orbital (1:1) planetary resonances during gas-driven orbital migration, *MNRAS*, **442**(2), p 2296.
- [33] Páez, R.I., Efthymiopoulos, C., (2015) Trojan resonant dynamics, stability, and chaotic diffusion, for parameters relevant to exoplanetary systems, *Celest. Mech. Dyn. Astron.*, **121**(2), p 139.
- [34] Páez, R.I., Locatelli, U., (2015) Trojan dynamics well approximated by a new Hamiltonian normal form, *MNRAS* **453**(2), p 2177.
- [35] Páez, R.I., Locatelli, U., Efthymiopoulos, C. (2016) *Celest.Mech.Dyn.Astron* **126**, p 519
- [36] Páez, R.I. (2016) New normal form approaches adapted to the Trojan problem - Ph.D. Thesis, *arXiv:1703.08819*
- [37] Robutel, P., Gabern, F., (2006) The resonant structure of Jupiter's Trojan asteroids - I. Long term stability and diffusion, *MNRAS* **372**, p 1463.
- [38] Schwarz, R., Süli, Á., Dvorak, R., Pilat-Lohinger, E., (2009) Stability of Trojan planets in multiplanetary systems, *Celest. Mech. Dyn. Astron.* **104**, p 69.
- [39] Tsiganis, K., Varvoglis, H., Dvorak, R., (2005) Chaotic diffusion and effective stability of Jupiter Trojans, *Celest. Mech. Dyn. Astron.* **92**, p 71.
- [40] Voglis, N., Efthymiopoulos, C., (1998) Angular dynamical spectra. A new method for determining frequencies, weak chaos and cantori *J. Phys. A* **31**, p. 2913.